

Differential cardiovascular effects of nano- and micro-particles in mice: Implications for ultrafine and fine particle disease burden in humans

Marin Kuntic^{1,2}, Ivana Kuntic¹, Dirk Cleppien³, Andrea Pozzer⁴, David Nußbaum¹, Matthias Oelze¹, Tristan Junglas¹, Lea Strohm¹, Henning Ubbens¹, Steffen Daub¹, Maria Teresa Bayo Jimenez¹, Sven Dankwardt^{2,5,6}, Thomas Berkemeier⁷, Omar Hahad^{1,2}, Matthias Kohl⁴, Sebastian Steven^{1,5,8}, Albrecht Stroh^{3,9}, Jos Lelieveld⁴, Thomas Münzel^{1,2}, Andreas Daiber^{1,2,5*}*

¹ University Medical Center Mainz, Department for Cardiology 1, Molecular Cardiology, Mainz, Germany

² German Center for Cardiovascular Research (DZHK), Partner Site Rhine-Main, Mainz, Germany

³ Leibniz-Institut für Resilienzforschung (LIR) gGmbH, Mainz Animal Imaging Center (MAIC), Mainz, Germany

⁴ Max Planck Institute for Chemistry, Atmospheric Chemistry Department, Mainz, Germany

⁵ Center for Thrombosis and Hemostasis (CTH), University Medical Center of the Johannes Gutenberg-University, Mainz, Germany

⁶ University Medical Center Ulm, Department of Clinical Chemistry, Ulm, Germany

⁷ Max Planck Institute for Chemistry, Multiphase Chemistry Department, Mainz, Germany

⁸ Division of Cardiology, Goethe University Frankfurt, University Hospital, Department of Medicine III, Frankfurt a. M., Germany

⁹ University Medical Center Mainz, Institute of Pathophysiology, Mainz, Germany

Running title: Micro- and nano-PM distribution and cardiovascular effects

* These authors contributed equally and are joint senior authors.

Address correspondence to:

Prof. Dr. Andreas Daiber

University Medical Center of the Johannes Gutenberg-Universität Mainz, Department of Cardiology 1, Mainz, Germany

Phone +49 (0)6131 176280, E-mail: daiber@uni-mainz.de

Word count without legends and references: 5692 + 1800 for figures

Total word count: 10296

References: 81

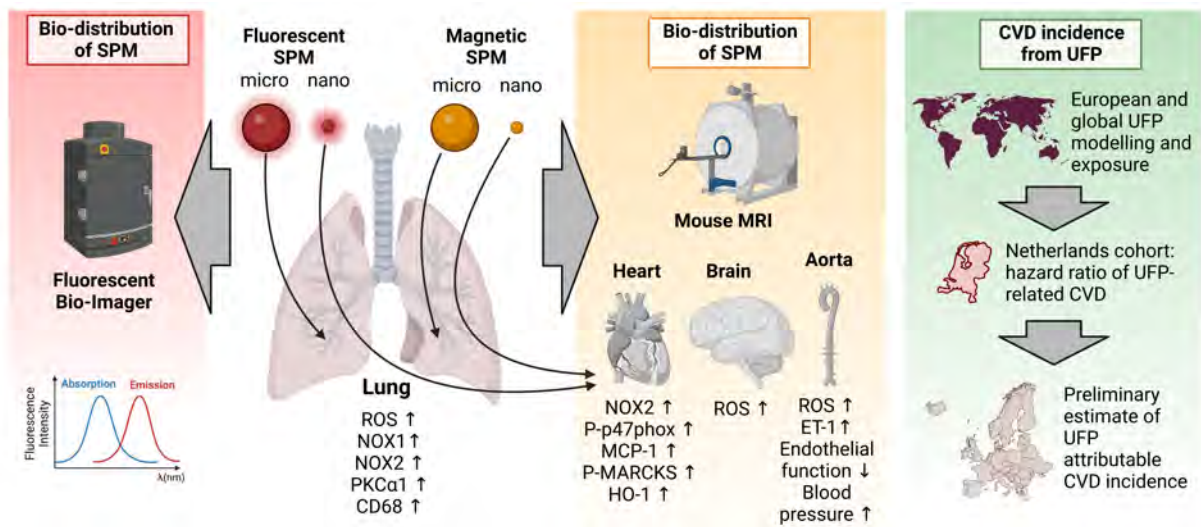
Figures: 7

ABSTRACT (244 words)

Particulate matter (PM) air pollution presents a major environmental and public health challenge because of its non-uniform size distribution and chemical composition. Air quality regulations generally categorize particulate matter (PM) size into PM₁₀, PM_{2.5}, and ultrafine particles (UFPs) with aerodynamic diameters < 10, 2.5, and 0.1 μm, respectively. We examined the differential impact of particle size per se on selected organ systems using a custom whole-body mouse exposure system using synthetic PM (SPM). The micrometer-sized SPM accumulated in the lungs as the primary entry organ, while ultrafine SPM showed less accumulation, implying a transition into circulation. Micro SPM-exposed mice exhibited inflammation and NADPH oxidase-derived oxidative stress in the lungs. Ultrafine SPM-exposed mice did not show oxidative stress in the lungs but rather at the brain, heart, and vasculature levels. Endothelial dysfunction and blood pressure increase were more pronounced in ultrafine SPM exposed mice, supported by increased endothelin-1 and decreased endothelial nitric oxide synthase expression, enhancing constriction and reducing vasodilation. To derive a preliminary estimate of the cardiovascular disease burden of UFPs in humans, we used new high-resolution exposure data at a global scale, and applied hazard ratios from an epidemiological cohort study. We derived a UFP-associated incidence of 419 (95% CI 78–712) thousand cardiovascular disease cases per year in the European Union and 5.6 (95% CI 1.1–9.3) million globally. This work provides novel insights into the different toxicological profiles of inhaled ultrafine particles and public health consequences of exposure, guiding future studies.

KEYWORDS: Particulate matter; size-dependent effects; oxidative stress; inflammation; UFP model; cardiovascular disease.

GRAPHICAL ABSTRACT



INTRODUCTION

Air pollution is a major contributor to non-communicable diseases¹. The Global Burden of Disease study ranks air pollution among the leading risk factors for mortality and disability-adjusted life years (DALYs)², with annual excess mortality estimates ranging from 8.7 million³ to 10.2 million⁴. Particulate matter (PM), a significant component of air pollution, is particularly harmful⁵. PM includes all solid and liquid particles in the air^{6,7} and varies in sources, structure, composition, and size. PM's composition depends on its origin (naturally or anthropogenic) and environmental interactions^{8,9}. PM is commonly classified by diameter: PM₁₀ (<10 µm), PM_{2.5} (<2.5 µm), and ultra-fine particles (UFP, <0.1 µm)¹⁰, with most health studies and regulations focusing on the mass concentrations of PM₁₀ and PM_{2.5}¹¹. Research done during the last two decades revealed the difference in toxicity between PM₁₀ and PM_{2.5}, as the larger particles do not penetrate as deeply into the respiratory tract and are more easily eliminated¹²⁻¹⁴. It is important to remember that PM₁₀, on its own, still presents a significant risk factor for many diseases¹⁵, probably also due to loading with environmental toxins. The health differences between UFP and PM_{2.5} remain understudied, and only a few cohort studies have been reported. This is mainly because UFP were, until recently, not routinely measured in air pollution networks.

Ambient PM typically has a mineral or carbon core and carries chemicals like inorganic salts, organic compounds, transition and heavy metals, and endotoxins^{8,16,17}. However, measuring PM size and number concentrations is more straightforward and less expensive than composition differentiation, especially for particles in the PM_{2.5} and PM₁₀ size ranges¹⁸. Accordingly, PM_{2.5} and PM₁₀ mass concentrations (in µg/m³) are widely adopted parameters in health studies and regulations, while UFP mass concentrations are less commonly measured and used^{19,20}. Smaller particles tend to be more harmful than larger particles, and research often focuses on PM_{2.5} over PM₁₀^{10,21}. UFPs are considered especially detrimental, likely due to their ability to penetrate the air-blood barrier^{22,23}. While UFPs often dominate ambient particle size distributions by number, they only comprise a small fraction of PM_{2.5} mass²⁴. Thus, using PM_{2.5} or PM₁₀ mass concentrations as a predictor for health endpoints not only disregards the composition of particles but also the differential toxicity of particle sizes within PM. While smaller particles contribute comparatively little to mass concentrations, they may be disproportionately more harmful. While previous large clinical studies often excluded UFP health effects since reliable quantification of

nanoparticles represented a challenge, recent technological innovations and more affordable devices now enable UFP measurement more broadly.

A study from China showed that only particles smaller than 1 μm (PM_1) are positively associated with cardiovascular morbidity²⁵. Another study from China demonstrated a positive association between PM in the size range of 0.25 – 0.5 μm and cardiovascular mortality while observing no significant association with mortality from respiratory diseases²⁶. A study in Erfurt, Germany, found a similarly higher risk for cardiovascular mortality from UFP compared to respiratory mortality²⁷. The results of these two studies support the transmigration of nano-sized particles through the lung and direct damage to remote organs. A recent study in Copenhagen, Denmark, established that hospital admissions for cardiovascular and respiratory diseases positively correlated with an increase in UFP concentrations²⁸. Interestingly, after adjustment for $\text{PM}_{2.5}$ all associations with respiratory diseases decreased, while associations with cardiovascular disease increased, pointing to a direct effect of UFP, but not of larger PM, on the cardiovascular system. Data from a Dutch cohort corroborate the findings of cardiovascular disease association with UFP rather than coarser PM, highlighting this through a two-pollutant model where UFP remained the only positively associated variable for cardiovascular risk²⁹. On the other hand, in a cohort from Toronto, Canada, no change in the association between UFP and acute myocardial infarction and congestive heart failure was observed after correcting for exposure to $\text{PM}_{2.5}$ and NO_2 ³⁰, and this was confirmed by another study on airborne nanoparticle concentrations reporting an association with increased mortality risk in Canada's two largest cities³¹. The European Study of Cohorts for Air Pollution Effects (ESCAPE) also found no correlation between $\text{PM}_{2.5}$ concentrations and all cardiovascular disease deaths³².

There is substantial epidemiological and clinical evidence for a major contribution of PM to adverse human health effects, and that not only the respiratory system is affected, but remote organ systems as well³³. Numerous studies have been conducted on the differential effects of the PM composition, providing an overview of the role and contribution of different toxicants carried by airborne PM³⁴⁻³⁶. On the other hand, the studies addressing the effects of PM size have been inconclusive. The reasons are the focus on air pollution-derived UFP that exhibits a high load-to-mass ratio of surface toxicants, which impedes detection of size effects¹⁰. Further, the use of biologically inert PM, e.g. for contrast agents, drug delivery systems and food or cosmetic stabilizers has generated contradicting findings^{37, 38}. Especially in preclinical research,

chemically inert particles, such as TiO₂, silver, gold, or synthetic carbon/plastic particles have been used³⁹⁻⁴¹.

This study aimed to determine if ultrafine or nanoparticles penetrate the air-blood barrier more easily than microparticles and if they can be detected in remote organs. We also sought reliable functional and molecular markers related to cardiovascular and pulmonary systems to differentiate the level of harm and tissue transmigration between particle sizes. Hazard ratios from a Dutch cohort were used to extrapolate UFP effects on cardiovascular disease incidence in humans, highlighting the importance of nanometer-sized particles in disease outcomes.

RESULTS AND DISCUSSION

With the present studies, we investigated the biological toxicity of nano- versus micro-sized synthetic particles with emphasis on their potential to transmigrate through the lung epithelium into the bloodstream and to cause damage to other remote organs (e.g. the aorta, heart, and brain). We used fluorescence-labeled or magnetic nano- versus micro-sized particles to trace their biodistribution. In the second part we estimated UFP effects on human cardiovascular disease incidence at a global scale.

Organ distribution of PM

The size distributions of the used SPM are presented in **suppl. Figure S2**. Since particle mass is proportional to the diameter cubed, when exposing animals to the same mass concentration, they are exposed to more individual particles in the nano SPM exposure categories.

After the exposure to fluorescent micro- or nano SPM, mice were sacrificed and extracted lungs were imaged with a fluorescence imager (**Figure 1A, B**). The lungs of mice exposed to micro SPM showed a pronounced difference in fluorescence when compared to non-exposed mice, while lungs of nano SPM exposed mice showed a more subtle increase in fluorescence intensity (**Figure 1A**). The more pronounced increase in fluorescence intensity after the micro SPM

exposure points to the accumulation of the particles in the lung, while the lower fluorescence after nano SPM exposure points to the migration of particles from the lung tissue into circulation.

After the exposure to magnetic micro or nano SPM, mice were subjected to a whole-body rodent MRI depicting the abdomen of the mice (**Figure 1C, D**). The T_2^* relaxation values of the tissue were measured, enabling the calculation of R_2^* parameter maps. We hypothesized that the iron particles may accumulate in the heart (**Figure 1E**) and liver (**Figure 1F**) when they enter the body, and therefore these organs were examined for contrast changes due to the presence of magnetic SPM. No statistically significant changes were observed in either organ, although a trend toward a reduction in R_2^* values was observed in the nano SPM exposed mice.

Using synthetic particles, i.e. free from detrimental air pollutants, we show that the size of PM plays a significant role in detrimental effects on multiple organ systems. This suggests additive or synergistic adverse effects by small particle size and a high load of toxicants due to high surface/mass ratio combined with high particle number concentrations^{23, 42}. Ambient particles contain chemically active substances (such as transition and heavy metals, peroxides, quinones, endotoxins) known to induce inflammation and oxidative stress⁴³⁻⁴⁷. The limitations applying for our animal studies, e.g. particle size distribution, sufficient concentrations for MRI contrast, are explained in detail in the **online supplement**.

Vascular function in nano- and micro SPM exposed mice

Systolic blood pressure, as measured by the tail-cuff method, was increased after exposure to both the fluorescent and magnetic nano SPM (**Figure 2A, C**). Blood pressure was not changed after the exposure to fluorescent and magnetic micro SPM. Endothelium-dependent vascular relaxation achieved through ACh titration showed a right shift after exposure to fluorescent nano SPM but not after the exposure to fluorescent micro SPM (**Figure 2B**). The endothelium-independent vascular relaxation in response to nitroglycerin was not changed upon fluorescent SPM exposure. The exposure to both magnetic nano and micro SPM caused a right shift in the endothelium-dependent relaxation curve by trend, but no clear pattern emerged (**Figure 2D**). The exposure to magnetic SPM also did not affect the endothelium-independent vascular relaxation in response to nitroglycerin. Aortic protein expression of endothelin 1 (ET-1) was also increased in

mice exposed to the magnetic nano SPM, together with a decrease in endothelial nitric oxide synthase (eNOS) by trend (**Figure 2E, F**).

The elevated levels of ROS in the aortic tissue that were observed after exposure to nano-sized SPM correlate with the impairment of endothelium-dependent vasodilation and the lowering of eNOS expression by trend. Elevation of ET-1 expression, a potent vasoconstrictor that is upregulated by oxidative stress⁴⁸, points to the ability of nano-sized PM to promote vascular dysfunction. Another pathway by which PM can influence the cardiovascular system is by activation of the sympathetic nervous system (SNS) and the amygdala stemming from the translocation of the UFPM through the olfactory nerve⁴⁹. The activation of the SNS leads to the release of catecholamines which cause vascular constriction, blood pressure increase and vascular inflammation^{50, 51}, also observed here together with the increase in cortical ROS production. In addition, modulation of the SNS can lead to disruption of the circadian rhythm, further disrupting cardiovascular redox balance by phase shifts of genes encoding for ROS producing and degrading proteins⁵². In addition, air pollutants cause circadian rhythms impairment by adverse redox regulation of the clock core components such as period, cryptochrome, clock and BMAL1. It was also previously observed that SPM can disrupt cardiac function through myocardial injury and apoptosis via ROS⁵³.

Oxidative stress in different tissues of PM exposed mice

Dihydroethidium (DHE) staining was used to assess spatial oxidative stress levels in aortic, pulmonary, and cortical tissue of SPM-exposed mice. Fluorescent nano SPM showed a significant increase in oxidized DHE-derived fluorescence in both aortic and cortical tissue (**Figure 3A, B**). The fluorescent micro SPM did not change the oxidative stress status in these tissues compared to the non-exposed control. Magnetic nano SPM exposure caused again increased oxidized DHE fluorescence signal (**Figure 3C, D**), which was absent upon exposure to magnetic micro SPM. In the pulmonary tissue, the magnetic micro and nano SPM showed an increase in oxidized DHE-derived fluorescence (**Figure 3E**). The lung tissue of fluorescent SPM-exposed animals could not be evaluated due to excessive fluorescence background originating from the accumulation of fluorescent particles in the lungs of exposed mice.

Oxidative stress and inflammation play a major role in vascular dysfunction as they interfere with the important pathways regulating vascular tone. Nitric oxide ($\cdot\text{NO}$), as an important signaling molecule, is susceptible to oxidative stress, as the reaction with superoxide ($\cdot\text{O}_2^-$) not only creates peroxynitrite (ONOO^-) at the expense of $\cdot\text{NO}$, but it also impairs $\cdot\text{NO}$ production by uncoupling eNOS^{7, 48}. Here the origin of $\cdot\text{O}_2^-$ can be attributed to the activation of the NADPH oxidase (NOX1/2), which is also supported by the elevation of the PKC activity through phosphorylation of MARCKS.

Protein markers of oxidative stress and inflammation in cardiac and pulmonary tissue

NADPH oxidase subunits NOX1 and NOX2 protein expression was elevated in lung tissue of magnetic micro SPM, but not in the lung tissue of nano SPM exposed mice (**Figure 4A, B**). In addition, the NADPH oxidase subunit p67phox was measured but did not show a trend in either micro or nano SPM exposure groups (**Figure 4C**). Protein kinase C alpha 1 ($\text{PKC}\alpha 1$), which promotes NADPH oxidase complex formation, was also elevated in the lung tissue but phosphorylated myristoylated alanine-rich C-kinase substrate (P-MARCKS), a marker of $\text{PKC}\alpha 1$ activity, was not changed (**Figure 4D, E**). CD68 was also elevated in the lungs of micro SPM-exposed mice, indicating local inflammation initiation (**Figure 4F**).

In cardiac tissue, it was the nano SPM that produced a significant effect. NADPH oxidase subunit NOX2 and the phosphorylated p47phox showed a significant increase in protein expression (**Figure 5A, B**), pointing to the activation of the ROS-producing complex. Monocyte chemoattractant protein-1 (MCP-1), a marker of inflammation, was also elevated in the cardiac tissue of nano SPM, but not the micro SPM exposed mice (**Figure 5C**). P-MARCKS' expression was increased upon nano SPM exposure, indicating kinase activity (**Figure 5D**). Heme oxygenase 1 (HO-1) was significantly upregulated in the hearts of both nano and micro SPM-exposed mice, indicating the activation of the antioxidant defense through the Nrf2 pathway (**Figure 5E**). The expression of dihydrofolate reductase (DHFR), was not observed to be significantly changed (**Figure 5F**).

Inflammation also leads to the development of vascular dysfunction, e.g. by oxidative burst of activated leukocytes upon tight adhesion to the endothelium or infiltration into the vascular wall⁵⁴. Elevated levels of CD68 in the pulmonary tissue of micro-sized SPM point to local

inflammation in the lung, which is also accompanied by increase in ROS production, while increased expression of MCP-1 in the cardiac tissue of nano-sized SPM point to the ability of these ultrafine particles to transmigrate through the lung epithelium, reach the circulation and to cause inflammation and remote organ damage, e.g. in the cardiovascular system.

Global exposure to UFP

Potential cardiovascular health impacts of ambient levels of UFP were also studied by combining exposure data with results from an epidemiological cohort study. **Figure 6A** presents the country-level, mean, and population-weighted exposure to UFP, aggregated from the downscaled data available at a spatial resolution of 0.1° latitude and longitude. The time period considered is one year for which coincident emission inventories and measurement data were available, based on recently published results⁵⁵. We concentrate on long-term –rather than acute– exposure because chronic oxidative stress and inflammatory responses are associated with cardiovascular, cardiometabolic, and cerebrovascular diseases⁵⁶. We find that countries with the highest exposure are found in the Middle East and some parts of Asia, to a large degree associated with a high degree of urbanization. Annual and country mean concentrations reach up to 20,000 particles cm^{-3} , e.g., in Singapore, Arabian Gulf states, and Egypt, and somewhat lower (up to 11,000 cm^{-3}) in other Middle Eastern countries (e.g., Israel, Jordan), and South and East Asia. Exposure is also very high in South Africa, New Zealand, Australia, Mexico, and several South American, North African, and Eastern European countries. In Europe, country and annual mean UFP exposure ranges from about 2,000–3,000 cm^{-3} in Scandinavia, 10,000 cm^{-3} in Balkan states, and 4,000–6,000 cm^{-3} in Western and Central Europe.

CVD incidence from UFP

We combined the downscaled UFP exposure data (0.1° resolution) with hazard ratios of the increased risk for incident CVD adopted from an epidemiological cohort study²⁹ and computed the attributable fractions as a function of UFP number concentrations. Results are shown in **Figure 7**. The cohort study was performed in the Netherlands, and considering it is the only one of its kind, we assume it is representative of conditions and the population in Europe. For the 27 countries of the European Union (EU-27) we estimate a UFP-attributable CVD incidence of 419

(95% CI: 78–712) thousand per year for a total population of 446 million. The highest incidence occurs in Germany, with 82 (15–142) thousand per year, followed by Italy with 67 (13–115) and France with 42 (8–71) thousand per year. Since these are relatively populous countries in the EU-27, we additionally estimated the per capita incidence and found that it is highest in Greece, with 171 (37–256) per 100,000 population per year, followed by Hungary, with 165 (34–253) and Bulgaria with 159 (30–267) per 100,000 annually, whereas it is lowest in Ireland with 33 (7–53) and Finland with 43 (8–74) per 100,000 population per year.

If the Dutch cohort study would also be representative worldwide (absent dedicated cohort studies), we derive a yearly global CVD incidence of 5.6 (95% CI: 1.1–9.3) million, attributable to the exposure to UFP (**Figure 7**). Since the global CVD incidence from all causes is 47.1 (95% UI: 40.9–53.9) million per year², the UFP-attributable incidence amounts to a fraction of about 11–12% of the total. **Figure 6B** shows these estimated fractions for all countries worldwide, suggesting particularly relevant implications for CVD incidence from UFP exposure in Middle Eastern and South Asian countries, for example. These results should be considered preliminary, i.e., first-order estimates until additional epidemiological studies become available that account for air pollution, including UFP, and health conditions in representative regions of the world. The annual global mean per capita CVD incidence due to UFP is estimated at 76.2 (95% UI: 16.2–115.2) per 100,000 population. CVD is the globally leading cause of death, amounting to 18.6 (95% UI: 17.1–19.7) million per year, nearly one-third of the all-cause mortality⁵⁷. By further hypothesising that CVD incidence is proportional to CVD mortality, we estimate that 2.0 (95% UI: 0.4–3.3) million CVD-related deaths per year could potentially be attributable to UFP exposure.

Our European and global estimates of UFP exposure and potential consequences for CVD incidence are preliminary and associated with uncertainties. The annual average UFP concentration in the cohort study of Downward et al. (2018)²⁹, performed among residents of major metropolitan areas in the Netherlands, was 11,110 ($\pm 2,400$) particles cm^{-3} . This is at the higher end of that observed in European cities (e.g., between Milan and Barcelona) but lower than in Chinese cities and Arabian Gulf states, for example^{58, 59}. It captures a good part but not the full spread we find in global, annual UFP exposure, and clearly, additional cohort studies are needed to reduce uncertainty. This applies to high-income but especially also to low- and middle-income countries. Even though the Downward et al. (2018)²⁹ study is the only one available that

directly attributes CVD incidence to UFP, it should be noted that these outcomes are qualitatively consistent with epidemiological studies that relate UFP to hypertension and diabetes^{60, 61} and congestive heart failure and acute myocardial infarction⁶², as well as enhanced mortality risk⁶³. Hence, the quantitative outcomes presented here may be uncertain, but there is still a high likelihood that exposure to UFP contributes to CVD incidence.

CONCLUSIONS

Our study highlights the distinct biological impacts of nano- and micro-sized synthetic particles in exposed mice, indicating effects on human health. Nano-sized particles can transmigrate through lung epithelium into the bloodstream, affecting distant organs such as the aorta, heart, and brain. This suggests significant direct systemic impacts, extending beyond the pulmonary effects typically associated with larger micro-sized particles, which tend to remain in the respiratory system, primarily causing pulmonary damage with localized and possible indirect systemic health outcomes. Our preliminary assessment based on data of human exposure to air pollution corroborates the detrimental health potential of UFP by their substantial contribution to the cardiovascular disease burden at the European and global scale.

Our data show that particles with a small diameter (in our study $SPM_{0.25}$) enhance the oxidative stress and inflammatory parameters in remote organ systems, while particles with larger diameters (in our study $SPM_{2.1}$ and $SPM_{4.1}$) impact the pulmonary system. This distinction is important in defining future studies, as different organ systems could be impacted by PM of varying sizes through different mechanisms, also leading to differential increase in the risk of specific disease categories, notably cardiovascular versus respiratory diseases, as supported by several clinical/epidemiological studies on UFP exposure–health associations. Our preliminary assessment based on data of human exposure to air pollution corroborates the detrimental health potential of UFP by their substantial contribution to the cardiovascular disease burden at the European and global scale.

Clinically, these findings emphasize the need for healthcare frameworks to consider particle size in air pollution regulations and health risk assessments. The ability of nano-sized particles to cause systemic harm underscores their potential role in exacerbating cardiovascular conditions and necessitates targeted public health strategies to mitigate their effects. Future regulatory measures should account for the unique risks posed by ultrafine particles, including revising air

quality standards to better reflect the cardiovascular health risks. This warrants the comprehensive addition of UFP measurements to air quality monitoring stations so that higher spatial and temporal resolution exposure maps can be developed to study epidemiological associations derived from large cohorts.

METHODS

Exposure of laboratory animals

All animals were treated following the Guide for the Care and Use of Laboratory Animals as adopted by the U.S. National Institutes of Health, and approval was granted by the Ethics Committee of the University Medical Center Mainz and the Landesuntersuchungsamt Rheinland-Pfalz (Koblenz, Germany; permit number: 23 177-07/G 20-1-055). All mice were housed under a 12-hour light/dark cycle in the ventilated animal cabinet and fed ad libitum. Male C57BL/6 mice, 8-12 weeks old, were exposed to either fluorescent particles or magnetic particles of two different sizes each or fresh air. The exposure lasted for 6 hours per day for 3 days. The average concentration of all synthetic particulate matter (SPM) in the exposure chamber was $230 \pm 46 \mu\text{g}/\text{m}^3$. The custom exposure system (described in detail in ⁶⁴) was acquired from TSE Systems GmbH (Hochtaunuskreis, Germany). Fluorescent SPM were acquired from Spherotec (Lake Forest, IL, US), nano SPM (FP-0256-2, Nile Red, 0.25 μm , polystyrene) and micro SPM (FP-2065-2, Nile Blue, 2.16 μm , polystyrene). Magnetic SPM were acquired from Kisker Biotech GmbH (Steinfurt, Germany), nano SPM (PMSI-H-.25-5, superparamagnetic silica-encapsulated FeO_x particles, 0.25 μm), micro SPM (PM4.5, magnetic polystyrene-encapsulated FeO_x particles, 4.13 μm). The particles were suspended in CLRwater and placed in the collision nebulizer of the exposure system. After nebulizing into an aerosol, the particle suspension droplets passed through a drying column and dry particles entered the exposure chamber. The mass concentration of SPM was monitored by a particle detector that consists of two instruments for different particle size ranges combined into a NanoSpectroPan instrument (TSE Systems GmbH, Germany). The electric field mobility spectrometer measured the particles in the size range from 0 to 0.2 μm , and the light scattering detector measured in the 0.2 – 35 μm range. The measured values of the mean SPM mass concentration in the exposure chamber were: $248 \pm 66 \mu\text{g}/\text{m}^3$ for nano-fluorescent

SPM, $270 \pm 65 \mu\text{g}/\text{m}^3$ for micro-fluorescent SPM, $209 \pm 37 \mu\text{g}/\text{m}^3$ for nano-magnetic SPM and $221 \pm 27 \mu\text{g}/\text{m}^3$ for micro-magnetic SPM.

The PM concentration range was chosen because $200 - 300 \mu\text{g}/\text{m}^3$ is a peak concentration reached in the most polluted cities^{65,66}, therefore it represents a good starting point for acute PM effect observations. The relation between mouse exposure and human exposure is approximately similar. Mice are exposed for only 6 hours per day, giving a $\frac{1}{4}$ of the total daily exposure, which is in line with the whole day exposures done previously^{67,68}. Mice have a respiratory rate of $80-230 \text{ min}^{-1}$ ⁶⁹ and tidal volume of 0.2 mL ⁷⁰, making the total mass of PM being inhaled during a 6 hour exposure session (approximate chamber concentration of $200 \mu\text{g}/\text{m}^3$) $1.15-3.31 \mu\text{g}$ (assuming 100 % PM retention). Assuming the mouse weight of 25 g, the 6 hour exposure session will result in $46-132 \mu\text{g}/\text{kg}/\text{day}$. Human respiratory rate is approximately $10-20 \text{ min}^{-1}$ and the tidal volume is approximately 0.5 L. Assuming the body mass of 60 kg and the same exposure of $200 \mu\text{g}/\text{m}^3$, a human would inhale $24-48 \mu\text{g}/\text{kg}/\text{day}$. Mouse exposure occurs during sleeping phase when the respiratory activity is in the lower range, we may assume that mouse and human exposures are on par.

After the exposure mice were sacrificed by transection of the diaphragm and removal of the heart and thoracic aorta under deep ketamine/xylazine anesthesia (i.p. 120/16 mg/kg body weight), and tissues were harvested. The mouse exposure paradigm is shown in **suppl. Figure S1**.

Detection of fluorescent SPM in the isolated organs

After the exposure to fluorescent SPM, mice were sacrificed as described above and organs were excised. Removed organs were then imaged using the IVIS® Spectrum imaging system (PerkinElmer Inc, Waltham, MA, US)^{71, 72}. For nano SPM excitation filter at 500 nm and emission filter at 560 nm was used, and for micro SPM excitation filter at 570 nm and emission filter at 620 nm was used. The mean pixels intensity from the images was obtained with the ImageJ software and used in the statistical analysis.

Detection of iron oxide SPM in the whole body via MRI

After the exposure to iron oxide SPM, mice were sacrificed by isoflurane overdose and whole bodies were frozen at -80°C . Before the magnetic resonance imaging (MRI) measurement, depicting the signal decrease caused by changes in T_2^* related to accumulated iron particles in the investigated tissue^{73, 74}, mice were heated to 25°C and kept at that temperature through the measurement by using a rectal temperature probe coupled with a ventilation system to maintain body temperature and avoid T_2^* drifts caused by temperature changes (Model 1030, Small Animal Instruments Inc., Stony Brook, NY, USA). A 9.4 T small animal MRI system with a 0.7 T/m gradient system (Biospec 94/20, Bruker Biospin GmbH, Ettlingen, Germany) controlled by Paravision 6.0.1 software was used for the measurements. To image the abdomen of the mice, a linear whole-body volume transmitter coil combined with an anatomically shaped 4-channel receive-only coil array for the rat brain was used. A 3D multigradient echo pulse sequence (TE/TR = (3.5/ 800) ms; average = 2; flip angle = 50° ; TA = 1 h 9 min) was carried out, recording 9 echoes with echo spacing = 5 ms to visualize the T_2^* signal decay. Isotropic voxels were measured with resolution of $(0.25 \times 0.25 \times 0.25) \text{ mm}^3$ resulting in a $192 \times 128 \times 27$ volume covering a FOV of $48 \times 32 \times 6.75 \text{ mm}^3$. The R_2^* parameter value per voxel was calculated by fitting an exponential decay curve to the corresponding pixels resulting in a volume of R_2^* values (MATLAB, R2022a; MathWorks; Natick, Massachusetts, USA). The R_2^* relaxation values were used for quantification, as the iron oxide SPM function as contrast agents and lower the T_2^* in the tissue they are present in.

Exposure model and emissions for human studies

We applied a data-informed global atmospheric modelling method to compute the exposure to air pollutants. The model for atmospheric chemistry and climate (EMAC) used in this study was applied at a horizontal resolution of about 1.875° latitude and longitude, with 31 vertical levels up to 10 hPa (~ 30 km altitude)^{75, 76}. The anthropogenic emissions of trace gases and particles used as model input have been adopted from the Community Emission Data System (CEDS)⁷⁷. Source sectors include fossil energy production, industry, land transport, shipping, aviation, domestic energy use from solid biofuels, waste incineration, agriculture, solvent production and use. The CEDS emission data have been produced at a geographical resolution of 0.5° . In addition, we employed the Emissions Database for Global Atmospheric Research (EDGAR⁷⁸) at 0.1° resolution latitude and longitude for downscaling. The emission size spectrum of aerosol

particles depends on the source sectors, according to published work⁷⁹, and has been optimized according to size distribution measurements⁵⁵. A comprehensive evaluation of the modelled atmospheric dust, black and organic carbon, aerosol optical depth, and aerosol organic and inorganic compounds is presented previously⁷⁶.

Downscaling of UFP concentrations

Since the relatively coarse grid resolution of the EMAC model does not do justice to concentration gradients near strong sources of ultrafine particles (UFP), in particular of primary particles near areas with heavy traffic and industrial emission hotspots, we downscaled the simulation results in two steps, first to 0.5° and then to 0.1° latitude and longitude (~9 km at mid-latitudes). Observation-guided downscaling was achieved by redistributing the model grid box average UFP concentration according to the anthropogenic source sectors, available at higher resolution in the CEDS and EDGAR emission inventories⁵⁵. UFP results were evaluated against the measured number of particles in the size fraction 3 nm to 100 nm, the former based on the lower size limit of the measurements. A linear relationship between the observed and modelled particle number concentrations was applied to redistribute the particles toward the source areas, successively in the 0.5° and 0.1° inventories. Comparison of the results with long-term measured UFP concentrations at 60 measurement locations in Europe, India, China, North America and remote locations worldwide indicate good agreement⁵⁵. The logarithmic correlation coefficient is $r = 0.95$ (the linear $r = 0.99$), the slope of the linear fit is 1.022, and the root mean square log error is 0.43.

Estimation of health impacts

Incident cardiovascular disease (CVD), C , attributable to the long-term exposure to UFP at geographical coordinates x and y , $M(x,y)$, was calculated by:

$$M(x, y) = \sum_j AF_j[X(x, y)] \cdot C_j(x, y) \cdot P(x, y)$$

where j refers to the age category >25 years, and X is the concentration of UFP⁸⁰. AF is the attributable fraction of the CVD incidence due to exposure, and P is the population at the geographical coordinates, i.e., the 0.1° grid cells for which we computed UFP exposure. The incident CVD and population data have been adopted from the Global Burden of Disease². The

AF has been derived from the hazard ratio (HR) associated with exposure to UFP from data of a published cohort study⁸¹, which identified the increased risk of all incident CVD:

$$AF_j = (HR_j(UFP) - 1)/HR_j(UFP)$$

A log-normal exposure-response function was applied to describe the dependency of HR on the concentration of UFP, according to $HR_j = \exp(\beta \times X)$. The factor β was estimated from previous results⁸¹ by using an HR of 1.18 (95% confidence interval (CI): 1.03–1.34) per 10,000 particles cm^{-3} , obtaining $\beta = 1.6 \times 10^{-5}$ (95% CI: $2.9 \times 10^{-6} - 2.9 \times 10^{-5}$). Note that we did not apply a theoretical minimum risk exposure level – whether there is one is unknown. The 95% confidence intervals in all our results have been derived by adopting the ranges as previously described⁸¹.

Statistics

Where possible, the results are presented as bar graphs with individual values. Two-way ANOVA (with Tukey's correction for comparison of multiple means) was used for comparisons of concentration-relaxation curves. One-way ANOVA (with Tukey's post-hoc analysis for comparison of multiple means) was used for comparisons of all other data. All statistical analysis was performed in Prism for Windows, version 9. The numerical value of the p-value is either used directly or a star signifies a p-value < 0.05 that was considered as statistically significant. The number of replicates in the different assays may vary since not all animals were used in all assays.

All other methods (blood pressure, vascular function studies, oxidative stress measurement, protein expression analysis) are provided in the **online supplement**.

ASSOCIATED CONTENT

SUPPORTING INFORMATION

Methodological description of blood pressure, whole body fluorescence imaging, magnetic resonance imaging, vascular function studies, oxidative stress measurement, protein expression analysis, human exposure model and health effects. Suppl. Figure S1 shows the mouse exposure scheme. Suppl. Figure S2 shows the particle size distribution.

Data availability

All original data are provided in the main manuscript or in the online supplement. Raw data will be provided upon reasonable request by the corresponding author.

Author contributions

M.Ku. designed the study, conducted the exposure experiments, analyzed most data, wrote part of the manuscript; I.K. helped with exposure experiments, conducted blood pressure measurements and analyzed these data; D.C. conducted the MRI experiments and analyzed these data; A.P. conducted the human UFP exposure-CVD incidence modeling and analyzed these data; D.N. conducted the ROS measurements by DHE staining; M.O. analyzed DHE staining and protein expression data; T.J. helped with exposure experiments; L.S. did animal work and prepared tissues; H.U. did animal work and prepared tissues; S.Dau. critically revised the manuscript and acquired funding; M.T.B.J. did animal work and prepared tissues; S.Dan. helped with the whole body fluorescence imaging and critically revised the manuscript; T.B. made crucial contributions to the exposure protocols and critically revised the manuscript; O.H. critically revised the manuscript; M.Ko. conducted the human UFP exposure-CVD incidence modeling; S.St. critically revised the manuscript; A.S. helped to analyze the MRI data and critically revised the manuscript; J.L. helped to analyze the human UFP exposure-CVD incidence modeling data, wrote part of the manuscript and acquired funding; T.M. wrote part of the manuscript and critically revised the manuscript; A.D. designed the study, wrote part of the manuscript, critically revised the manuscript and acquired funding.

Funding Sources

A.D. and T.M. were supported by vascular biology research grants from the Boehringer Ingelheim Foundation for the collaborative research group “Novel and neglected cardiovascular risk factors: molecular mechanisms and therapeutics” and through continuous research support from Foundation Heart of Mainz (mostly dedicated to the purchase of the exposure system and to the salary of M.K.). I.K. and M.T.B.J. hold/held TransMed PhD stipends funded by the Boehringer Ingelheim Foundation. L.S. and H.U. hold TransMed PhD stipends funded by the Else-Kröner-Fresenius Foundation. S.St. holds an excellence stipend of the Else-Kröner-Fresenius Foundation (2021_EKES.04). T.J. holds a MD stipend funded by the Heart Foundation Mainz. T.M. is PI and A.D. and M.K., O.H. and S.D. are (Young) Scientists of the DZHK (German Center for Cardiovascular Research), Partner Site Rhine-Main, Mainz, Germany. Large instrument funding by the German Research Foundation (DFG, project 251892550 to S. Danckwardt). Work in the lab of S.D. is supported by the EU Horizon 2020 Innovative training network ‘Thromboinflammation in Cardiovascular disorders’ (TICARDIO, Marie Skłodowska-Curie grant agreement No 813409). The work was also supported by COST Action CA20121 (BenBedPhar) and the environmental network EXPOHEALTH funded by the state Rhineland-Palatinate, Germany.

Acknowledgements

We are indebted to Jörg Schreiner, Alexandra Rosenberger, Nicole Glas and Angelica Karpi for their expert technical assistance. Most of the protein data and DHE stainings are part of the medical doctorate thesis of David Nußbaum.

Conflict of interest

The authors have no conflict of interest to declare.

REFERENCES

1. Hahad, O.; Rajagopalan, S.; Lelieveld, J.; Sorensen, M.; Frenis, K.; Daiber, A.; Basner, M.; Nieuwenhuijsen, M.; Brook, R. D.; Munzel, T., Noise and Air Pollution as Risk Factors for Hypertension: Part I-Epidemiology. *Hypertension* **2023**, *80*, (7), 1375-1383.
2. Collaborators, G. B. D. R. F., Global burden of 87 risk factors in 204 countries and territories, 1990-2019: a systematic analysis for the Global Burden of Disease Study 2019. *Lancet* **2020**, *396*, (10258), 1223-1249.
3. Lelieveld, J.; Klingmüller, K.; Pozzer, A.; Pöschl, U.; Fnais, M.; Daiber, A.; Münzel, T., Cardiovascular disease burden from ambient air pollution in Europe reassessed using novel hazard ratio functions. *European heart journal* **2019**, *40*, (20), 1590-1596.
4. Vohra, K.; Vodonos, A.; Schwartz, J.; Marais, E. A.; Sulprizio, M. P.; Mickley, L. J., Global mortality from outdoor fine particle pollution generated by fossil fuel combustion: Results from GEOS-Chem. *Environmental research* **2021**, *195*, 110754.
5. Munzel, T.; Sorensen, M.; Gori, T.; Schmidt, F. P.; Rao, X.; Brook, J.; Chen, L. C.; Brook, R. D.; Rajagopalan, S., Environmental stressors and cardio-metabolic disease: part I-epidemiologic evidence supporting a role for noise and air pollution and effects of mitigation strategies. *Eur Heart J* **2017**, *38*, (8), 550-556.
6. Poschl, U.; Shiraiwa, M., Multiphase chemistry at the atmosphere-biosphere interface influencing climate and public health in the anthropocene. *Chemical reviews* **2015**, *115*, (10), 4440-75.
7. Daiber, A.; Kuntic, M.; Hahad, O.; Delogu, L. G.; Rohrbach, S.; Di Lisa, F.; Schulz, R.; Munzel, T., Effects of air pollution particles (ultrafine and fine particulate matter) on mitochondrial function and oxidative stress - Implications for cardiovascular and neurodegenerative diseases. *Arch Biochem Biophys* **2020**, *696*, 108662.
8. Munzel, T.; Gori, T.; Al-Kindi, S.; Deanfield, J.; Lelieveld, J.; Daiber, A.; Rajagopalan, S., Effects of gaseous and solid constituents of air pollution on endothelial function. *Eur Heart J* **2018**, *39*, (38), 3543-3550.
9. Leresche, F.; Salazar, J. R.; Pfothner, D. J.; Hannigan, M. P.; Majestic, B. J.; Rosario-Ortiz, F. L., Photochemical Aging of Atmospheric Particulate Matter in the Aqueous Phase. *Environ Sci Technol* **2021**, *55*, (19), 13152-13163.
10. Schraufnagel, D. E., The health effects of ultrafine particles. *Experimental & molecular medicine* **2020**, *52*, (3), 311-317.
11. Organization, W. H., *WHO global air quality guidelines: particulate matter (PM_{2.5} and PM₁₀), ozone, nitrogen dioxide, sulfur dioxide and carbon monoxide*. World Health Organization: 2021.
12. Lu, F.; Xu, D.; Cheng, Y.; Dong, S.; Guo, C.; Jiang, X.; Zheng, X., Systematic review and meta-analysis of the adverse health effects of ambient PM_{2.5} and PM₁₀ pollution in the Chinese population. *Environ Res* **2015**, *136*, 196-204.
13. Chen, J.; Hoek, G., Long-term exposure to PM and all-cause and cause-specific mortality: A systematic review and meta-analysis. *Environ Int* **2020**, *143*, 105974.
14. Zhao, Y.; Cheng, Z.; Lu, Y.; Chang, X.; Chan, C.; Bai, Y.; Zhang, Y.; Cheng, N., PM₁₀ and PM_{2.5} particles as main air pollutants contributing to rising risks of coronary heart disease: a systematic review. *Environmental Technology Reviews* **2017**, *6*, (1), 174-185.
15. Orellano, P.; Reynoso, J.; Quaranta, N.; Bardach, A.; Ciapponi, A., Short-term exposure to particulate matter (PM₁₀ and PM_{2.5}), nitrogen dioxide (NO₂), and ozone (O₃) and all-cause and cause-specific mortality: Systematic review and meta-analysis. *Environ Int* **2020**, *142*, 105876.
16. Kelly, F. J.; Fussell, J. C., Size, source and chemical composition as determinants of toxicity attributable to ambient particulate matter. *Atmospheric Environment* **2012**, *60*, 504-526.
17. Poschl, U., Atmospheric aerosols: composition, transformation, climate and health effects. *Angewandte Chemie* **2005**, *44*, (46), 7520-40.

18. Amaral, S. S.; De Carvalho, J. A.; Costa, M. A. M.; Pinheiro, C., An Overview of Particulate Matter Measurement Instruments. *Atmosphere* **2015**, *6*, (9), 1327-1345.
19. Pan, S. S.; Qiu, Y. T.; Li, M.; Yang, Z. Q.; Liang, D. P., Recent Developments in the Determination of PM_{2.5} Chemical Composition. *Bulletin of Environmental Contamination and Toxicology* **2022**, *108*, (5), 819-823.
20. Taiwo, A. M.; Beddows, D. C. S.; Shi, Z. B.; Harrison, R. M., Mass and number size distributions of particulate matter components: Comparison of an industrial site and an urban background site. *Science of the Total Environment* **2014**, *475*, 29-38.
21. Agency, U. E. P., Technical Assistance Document for the Reporting of Daily Air Quality – the Air Quality Index (AQI). In 2018.
22. Miller, M. R.; Raftis, J. B.; Langrish, J. P.; McLean, S. G.; Samutrtai, P.; Connell, S. P.; Wilson, S.; Vesey, A. T.; Fokkens, P. H. B.; Boere, A. J. F.; Krystek, P.; Campbell, C. J.; Hadoke, P. W. F.; Donaldson, K.; Cassee, F. R.; Newby, D. E.; Duffin, R.; Mills, N. L., Inhaled Nanoparticles Accumulate at Sites of Vascular Disease. *ACS Nano* **2017**, *11*, (5), 4542-4552.
23. Kwon, H. S.; Ryu, M. H.; Carlsten, C., Ultrafine particles: unique physicochemical properties relevant to health and disease. *Experimental & molecular medicine* **2020**, *52*, (3), 318-328.
24. Pozzer, A.; Anenberg, S. C.; Dey, S.; Haines, A.; Lelieveld, J.; Chowdhury, S., Mortality Attributable to Ambient Air Pollution: A Review of Global Estimates. *Geohealth* **2023**, *7*, (1), e2022GH000711.
25. Liu, L.; Breitner, S.; Schneider, A.; Cyrus, J.; Bruske, I.; Franck, U.; Schlink, U.; Marian Leitte, A.; Herbarth, O.; Wiedensohler, A.; Wehner, B.; Pan, X.; Wichmann, H. E.; Peters, A., Size-fractionated particulate air pollution and cardiovascular emergency room visits in Beijing, China. *Environ Res* **2013**, *121*, 52-63.
26. Meng, X.; Ma, Y.; Chen, R.; Zhou, Z.; Chen, B.; Kan, H., Size-fractionated particle number concentrations and daily mortality in a Chinese city. *Environ Health Perspect* **2013**, *121*, (10), 1174-8.
27. Stolzel, M.; Breitner, S.; Cyrus, J.; Pitz, M.; Wolke, G.; Kreyling, W.; Heinrich, J.; Wichmann, H. E.; Peters, A., Daily mortality and particulate matter in different size classes in Erfurt, Germany. *J Expo Sci Environ Epidemiol* **2007**, *17*, (5), 458-67.
28. Bergmann, M. L.; Andersen, Z. J.; Massling, A.; Kindler, P. A.; Loft, S.; Amini, H.; Cole-Hunter, T.; Guo, Y.; Maric, M.; Nordstrom, C.; Taghavi, M.; Tuffier, S.; So, R.; Zhang, J.; Lim, Y. H., Short-term exposure to ultrafine particles and mortality and hospital admissions due to respiratory and cardiovascular diseases in Copenhagen, Denmark. *Environ Pollut* **2023**, *336*, 122396.
29. Downward, G. S.; van Nunen, E.; Kerckhoffs, J.; Vineis, P.; Brunekreef, B.; Boer, J. M. A.; Messier, K. P.; Roy, A.; Verschuren, W. M. M.; van der Schouw, Y. T.; Sluijs, I.; Gulliver, J.; Hoek, G.; Vermeulen, R., Long-Term Exposure to Ultrafine Particles and Incidence of Cardiovascular and Cerebrovascular Disease in a Prospective Study of a Dutch Cohort. *Environmental health perspectives* **2018**, *126*, (12), 127007.
30. Bai, L.; Weichenthal, S.; Kwong, J. C.; Burnett, R. T.; Hatzopoulou, M.; Jerrett, M.; van Donkelaar, A.; Martin, R. V.; Van Ryswyk, K.; Lu, H.; Kopp, A.; Chen, H., Associations of Long-Term Exposure to Ultrafine Particles and Nitrogen Dioxide With Increased Incidence of Congestive Heart Failure and Acute Myocardial Infarction. *Am J Epidemiol* **2019**, *188*, (1), 151-159.
31. Lloyd, M.; Olaniyan, T.; Ganji, A.; Xu, J.; Venuta, A.; Simon, L.; Zhang, M.; Saeedi, M.; Yamanouchi, S.; Wang, A.; Schmidt, A.; Chen, H.; Villeneuve, P.; Apte, J.; Lavigne, E.; Burnett, R. T.; Tjepkema, M.; Hatzopoulou, M.; Weichenthal, S., Airborne Nanoparticle Concentrations Are Associated with Increased Mortality Risk in Canada's Two Largest Cities. *American journal of respiratory and critical care medicine* **2024**.
32. Beelen, R.; Stafoggia, M.; Raaschou-Nielsen, O.; Andersen, Z. J.; Xun, W. W.; Katsouyanni, K.; Dimakopoulou, K.; Brunekreef, B.; Weinmayr, G.; Hoffmann, B.; Wolf, K.; Samoli, E.; Houthuijs, D.; Nieuwenhuijsen, M.; Oudin, A.; Forsberg, B.; Olsson, D.; Salomaa, V.; Lanki, T.; Yli-Tuomi, T., et al.,

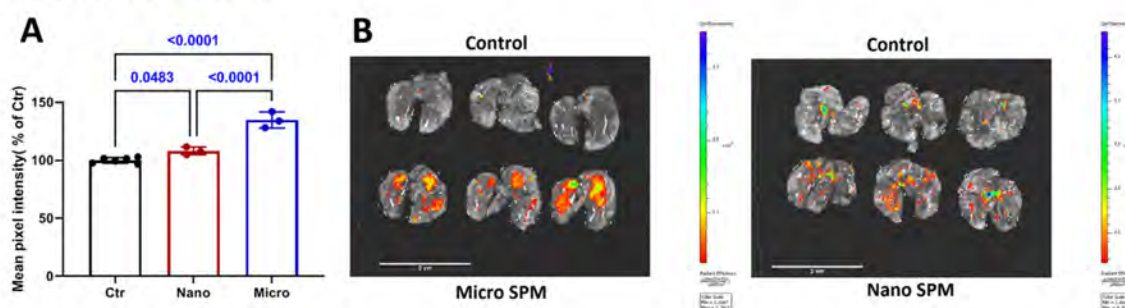
- Long-term exposure to air pollution and cardiovascular mortality: an analysis of 22 European cohorts. *Epidemiology* **2014**, *25*, (3), 368-78.
33. Lelieveld, J.; Klingmuller, K.; Pozzer, A.; Poschl, U.; Fnais, M.; Daiber, A.; Munzel, T., Cardiovascular disease burden from ambient air pollution in Europe reassessed using novel hazard ratio functions. *Eur Heart J* **2019**, *40*, (20), 1590-1596.
 34. Park, M.; Joo, H. S.; Lee, K.; Jang, M.; Kim, S. D.; Kim, I.; Borlaza, L. J. S.; Lim, H.; Shin, H.; Chung, K. H.; Choi, Y. H.; Park, S. G.; Bae, M. S.; Lee, J.; Song, H.; Park, K., Differential toxicities of fine particulate matters from various sources. *Scientific reports* **2018**, *8*, (1), 17007.
 35. Achilleos, S.; Kioumourtoglou, M. A.; Wu, C. D.; Schwartz, J. D.; Koutrakis, P.; Papatheodorou, S. I., Acute effects of fine particulate matter constituents on mortality: A systematic review and meta-regression analysis. *Environ Int* **2017**, *109*, 89-100.
 36. Araujo, J. A.; Nel, A. E., Particulate matter and atherosclerosis: role of particle size, composition and oxidative stress. *Part Fibre Toxicol* **2009**, *6*, 24.
 37. Murugadoss, S.; Lison, D.; Godderis, L.; Van Den Brule, S.; Mast, J.; Brassinne, F.; Sebaihi, N.; Hoet, P. H., Toxicology of silica nanoparticles: an update. *Arch Toxicol* **2017**, *91*, (9), 2967-3010.
 38. Winkler, H. C.; Suter, M.; Naegeli, H., Critical review of the safety assessment of nano-structured silica additives in food. *J Nanobiotechnology* **2016**, *14*, (1), 44.
 39. Yao, L.; Bojic, D.; Liu, M., Applications and safety of gold nanoparticles as therapeutic devices in clinical trials. *J Pharm Anal* **2023**, *13*, (9), 960-967.
 40. Srivastava, V.; Gusain, D.; Sharma, Y. C., Critical Review on the Toxicity of Some Widely Used Engineered Nanoparticles. *Industrial & Engineering Chemistry Research* **2015**, *54*, (24), 6209-6233.
 41. Hwang, J.; Choi, D.; Han, S.; Jung, S. Y.; Choi, J.; Hong, J., Potential toxicity of polystyrene microplastic particles. *Sci Rep* **2020**, *10*, (1), 7391.
 42. Chen, R.; Hu, B.; Liu, Y.; Xu, J.; Yang, G.; Xu, D.; Chen, C., Beyond PM_{2.5}: The role of ultrafine particles on adverse health effects of air pollution. *Biochim Biophys Acta* **2016**, *1860*, (12), 2844-55.
 43. Valacchi, G.; Magnani, N.; Woodby, B.; Ferreira, S. M.; Evelson, P., Particulate Matter Induces Tissue OxInflammation: From Mechanism to Damage. *Antioxid Redox Signal* **2020**, *33*, (4), 308-326.
 44. Liu, L.; Urch, B.; Szyszkowicz, M.; Evans, G.; Speck, M.; Van Huang, A.; Leingartner, K.; Shutt, R. H.; Pelletier, G.; Gold, D. R.; Brook, J. R.; Godri Pollitt, K.; Silverman, F. S., Metals and oxidative potential in urban particulate matter influence systemic inflammatory and neural biomarkers: A controlled exposure study. *Environ Int* **2018**, *121*, (Pt 2), 1331-1340.
 45. Arias-Perez, R. D.; Taborda, N. A.; Gomez, D. M.; Narvaez, J. F.; Porras, J.; Hernandez, J. C., Inflammatory effects of particulate matter air pollution. *Environ Sci Pollut Res Int* **2020**, *27*, (34), 42390-42404.
 46. Lakey, P. S.; Berkemeier, T.; Tong, H.; Arangio, A. M.; Lucas, K.; Poschl, U.; Shiraiwa, M., Chemical exposure-response relationship between air pollutants and reactive oxygen species in the human respiratory tract. *Scientific reports* **2016**, *6*, 32916.
 47. Lelieveld, S.; Lelieveld, J.; Mishra, A.; Daiber, A.; Pozzer, A.; Poschl, U.; Berkemeier, T., Endogenous Nitric Oxide Can Enhance Oxidative Stress Caused by Air Pollutants and Explain Higher Susceptibility of Individuals with Inflammatory Disorders. *Environmental science & technology* **2024**, *58*, (4), 1823-1831.
 48. Daiber, A.; Steven, S.; Weber, A.; Shuvaev, V. V.; Muzykantov, V. R.; Laher, I.; Li, H.; Lamas, S.; Munzel, T., Targeting vascular (endothelial) dysfunction. *Br J Pharmacol* **2017**, *174*, (12), 1591-1619.
 49. Block, M. L.; Elder, A.; Auten, R. L.; Bilbo, S. D.; Chen, H.; Chen, J. C.; Cory-Slechta, D. A.; Costa, D.; Diaz-Sanchez, D.; Dorman, D. C.; Gold, D. R.; Gray, K.; Jeng, H. A.; Kaufman, J. D.; Kleinman, M. T.;

- Kirshner, A.; Lawler, C.; Miller, D. S.; Nadadur, S. S.; Ritz, B., et al., The outdoor air pollution and brain health workshop. *Neurotoxicology* **2012**, *33*, (5), 972-84.
50. Hahad, O.; Bayo Jimenez, M. T.; Kuntic, M.; Frenis, K.; Steven, S.; Daiber, A.; Munzel, T., Cerebral consequences of environmental noise exposure. *Environ Int* **2022**, *165*, 107306.
51. Munzel, T.; Steven, S.; Hahad, O.; Daiber, A., The sixth sense is involved in noise-induced stress responses and vascular inflammation: evidence for heightened amygdalar activity in response to transport noise in man. *Eur Heart J* **2020**, *41*, (6), 783-785.
52. Daiber, A.; Frenis, K.; Kuntic, M.; Li, H.; Wolf, E.; Kilgallen, A. B.; Lecour, S.; Van Laake, L. W.; Schulz, R.; Hahad, O.; Munzel, T., Redox Regulatory Changes of Circadian Rhythm by the Environmental Risk Factors Traffic Noise and Air Pollution. *Antioxid Redox Signal* **2022**, *37*, (10-12), 679-703.
53. Qi, Y.; Xu, H.; Li, X.; Zhao, X.; Li, Y.; Zhou, X.; Chen, S.; Shen, N.; Chen, R.; Li, Y.; Sun, Z.; Guo, C., Silica nanoparticles induce cardiac injury and dysfunction via ROS/Ca(2+)/CaMKII signaling. *Sci Total Environ* **2022**, *837*, 155733.
54. Daiber, A.; Steven, S.; Euler, G.; Schulz, R., Vascular and Cardiac Oxidative Stress and Inflammation as Targets for Cardioprotection. *Curr Pharm Des* **2021**, *27*, (18), 2112-2130.
55. Kohl, M.; Lelieveld, J.; Chowdhury, S.; Ehrhart, S.; Sharma, D.; Cheng, Y. F.; Tripathi, S. N.; Sebastian, M.; Pandithurai, G.; Wang, H. L.; Pozzer, A., Numerical simulation and evaluation of global ultrafine particle concentrations at the Earth's surface. *Atmospheric Chemistry and Physics* **2023**, *23*, (20), 13191-13215.
56. Peters, A.; Nawrot, T. S.; Baccarelli, A. A., Hallmarks of environmental insults. *Cell* **2021**, *184*, (6), 1455-1468.
57. Roth, G. A.; Mensah, G. A.; Johnson, C. O.; Addolorato, G.; Ammirati, E.; Baddour, L. M.; Barengo, N. C.; Beaton, A. Z.; Benjamin, E. J.; Benziger, C. P.; Bonny, A.; Brauer, M.; Brodmann, M.; Cahill, T. J.; Carapetis, J.; Catapano, A. L.; Chugh, S. S.; Cooper, L. T.; Coresh, J.; Criqui, M., et al., Global Burden of Cardiovascular Diseases and Risk Factors, 1990-2019: Update From the GBD 2019 Study. *J Am Coll Cardiol* **2020**, *76*, (25), 2982-3021.
58. de Jesus, A. L.; Rahman, M. M.; Mazaheri, M.; Thompson, H.; Knibbs, L. D.; Jeong, C.; Evans, G.; Nei, W.; Ding, A.; Qiao, L.; Li, L.; Portin, H.; Niemi, J. V.; Timonen, H.; Luoma, K.; Petaja, T.; Kulmala, M.; Kowalski, M.; Peters, A.; Cyrus, J., et al., Ultrafine particles and PM(2.5) in the air of cities around the world: Are they representative of each other? *Environ Int* **2019**, *129*, 118-135.
59. Trechera, P.; Garcia-Marles, M.; Liu, X.; Reche, C.; Perez, N.; Savadkoobi, M.; Beddows, D.; Salma, I.; Vorosmarty, M.; Casans, A.; Casquero-Vera, J. A.; Hueglin, C.; Marchand, N.; Chazeau, B.; Gille, G.; Kalkavouras, P.; Mihalopoulos, N.; Ondracek, J.; Zikova, N.; Niemi, J. V., et al., Phenomenology of ultrafine particle concentrations and size distribution across urban Europe. *Environ Int* **2023**, *172*, 107744.
60. Bai, L.; Chen, H.; Hatzopoulou, M.; Jerrett, M.; Kwong, J. C.; Burnett, R. T.; van Donkelaar, A.; Copes, R.; Martin, R. V.; Van Ryswyk, K.; Lu, H.; Kopp, A.; Weichenthal, S., Exposure to Ambient Ultrafine Particles and Nitrogen Dioxide and Incident Hypertension and Diabetes. *Epidemiology* **2018**, *29*, (3), 323-332.
61. Lin, L. Z.; Gao, M.; Xiao, X.; Knibbs, L. D.; Morawska, L.; Dharmage, S. C.; Heinrich, J.; Jalaludin, B.; Lin, S.; Guo, Y. M.; Xu, S. L.; Wu, Q. Z.; Chen, G. B.; Yang, B. Y.; Zeng, X. W.; Yu, Y. J.; Hu, L. W.; Dong, G. H., Ultrafine particles, blood pressure and adult hypertension: a population-based survey in Northeast China. *Environmental Research Letters* **2021**, *16*, (9).
62. Bai, L.; Weichenthal, S.; Kwong, J. C.; Burnett, R. T.; Hatzopoulou, M.; Jerrett, M.; van Donkelaar, A.; Martin, R. V.; Van Ryswyk, K.; Lu, H.; Kopp, A.; Chen, H., Associations of Long-Term Exposure to Ultrafine Particles and Nitrogen Dioxide With Increased Incidence of Congestive Heart Failure and Acute Myocardial Infarction. *American Journal of Epidemiology* **2019**, *188*, (1), 151-159.

63. Pond, Z. A.; Saha, P. K.; Coleman, C. J.; Presto, A. A.; Robinson, A. L.; Arden Pope Iii, C., Mortality risk and long-term exposure to ultrafine particles and primary fine particle components in a national U.S. Cohort. *Environ Int* **2022**, *167*, 107439.
64. Kuntic, M.; Kuntic, I.; Krishnankutty, R.; Gericke, A.; Oelze, M.; Junglas, T.; Bayo Jimenez, M. T.; Stamm, P.; Nandudu, M.; Hahad, O.; Keppeler, K.; Daub, S.; Vujacic-Mirski, K.; Rajlic, S.; Strohm, L.; Ubbens, H.; Tang, Q.; Jiang, S.; Ruan, Y.; Macleod, K. G., et al., Co-exposure to urban particulate matter and aircraft noise adversely impacts the cerebro-pulmonary-cardiovascular axis in mice. *Redox biology* **2023**, *59*, 102580.
65. Michal Krzyzanowski, M.; Apte, J. S.; Bonjour, S. P.; Brauer, M.; Cohen, A. J.; Pruss-Ustun, A. M., Air Pollution in the Mega-cities. *Global Environmental Health and Sustainability* **2014**, *1*, 185–191.
66. Lv, B.; Cai, J.; Xu, B.; Bai, Y., Understanding the Rising Phase of the PM(2.5) Concentration Evolution in Large China Cities. *Scientific reports* **2017**, *7*, 46456.
67. Haghani, A.; Johnson, R.; Safi, N.; Zhang, H.; Thorwald, M.; Mousavi, A.; Woodward, N. C.; Shirmohammadi, F.; Coussa, V.; Wise, J. P., Jr.; Forman, H. J.; Sioutas, C.; Allayee, H.; Morgan, T. E.; Finch, C. E., Toxicity of urban air pollution particulate matter in developing and adult mouse brain: Comparison of total and filter-eluted nanoparticles. *Environ Int* **2020**, *136*, 105510.
68. Li, D.; Zhang, R.; Cui, L.; Chu, C.; Zhang, H.; Sun, H.; Luo, J.; Zhou, L.; Chen, L.; Cui, J.; Chen, S.; Mai, B.; Chen, S.; Yu, J.; Cai, Z.; Zhang, J.; Jiang, Y.; Aschner, M.; Chen, R.; Zheng, Y., et al., Multiple organ injury in male C57BL/6J mice exposed to ambient particulate matter in a real-ambient PM exposure system in Shijiazhuang, China. *Environ Pollut* **2019**, *248*, 874-887.
69. Committee, J. H. U. A. C. a. U. <https://web.jhu.edu/animalcare/procedures/mouse.html>
70. Tankersley, C. G.; Fitzgerald, R. S.; Levitt, R. C.; Mitzner, W. A.; Ewart, S. L.; Kleeberger, S. R., Genetic control of differential baseline breathing pattern. *Journal of applied physiology* **1997**, *82*, (3), 874-81.
71. Steven, S.; Jurk, K.; Kopp, M.; Kroller-Schon, S.; Mikhed, Y.; Schwierczek, K.; Roohani, S.; Kashani, F.; Oelze, M.; Klein, T.; Tokalov, S.; Danckwardt, S.; Strand, S.; Wenzel, P.; Munzel, T.; Daiber, A., Glucagon-like peptide-1 receptor signalling reduces microvascular thrombosis, nitro-oxidative stress and platelet activation in endotoxaemic mice. *Br J Pharmacol* **2017**, *174*, (12), 1620-1632.
72. Tokalov, S. V.; Bachiller, D., IV delivery of fluorescent beads. *Chest* **2012**, *141*, (3), 833-834.
73. Stroh, A.; Faber, C.; Neuberger, T.; Lorenz, P.; Sieland, K.; Jakob, P. M.; Webb, A.; Pilgrimm, H.; Schober, R.; Pohl, E. E.; Zimmer, C., In vivo detection limits of magnetically labeled embryonic stem cells in the rat brain using high-field (17.6 T) magnetic resonance imaging. *Neuroimage* **2005**, *24*, (3), 635-45.
74. Stroh, A.; Zimmer, C.; Werner, N.; Gertz, K.; Weir, K.; Kronenberg, G.; Steinbrink, J.; Mueller, S.; Sieland, K.; Dirnagl, U.; Nickenig, G.; Endres, M., Tracking of systemically administered mononuclear cells in the ischemic brain by high-field magnetic resonance imaging. *Neuroimage* **2006**, *33*, (3), 886-97.
75. Jöckel, P.; Tost, H.; Pozzer, A.; Kunze, M.; Kirner, O.; Brenninkmeijer, C. A. M.; Brinkop, S.; Cai, D. S.; Dyroff, C.; Eckstein, J.; Frank, F.; Garny, H.; Gottschaldt, K. D.; Graf, P.; Grewe, V.; Kerkweg, A.; Kern, B.; Matthes, S.; Mertens, M.; Meul, S., et al., Earth System Chemistry integrated Modelling (ESCiMo) with the Modular Earth Submodel System (MESSy) version 2.51. *Geoscientific Model Development* **2016**, *9*, (3), 1153-1200.
76. Pozzer, A.; Reifenberg, S. F.; Kumar, V.; Franco, B.; Kohl, M.; Taraborrelli, D.; Gromov, S.; Ehrhart, S.; Jöckel, P.; Sander, R.; Fall, V.; Rosanka, S.; Karydis, V.; Akritidis, D.; Emmerichs, T.; Crippa, M.; Guizzardi, D.; Kaiser, J. W.; Clarisse, L.; Kiendler-Scharr, A., et al., Simulation of organics in the atmosphere: evaluation of EMACv2.54 with the Mainz Organic Mechanism (MOM) coupled to the ORACLE (v1.0) submodel. *Geoscientific Model Development* **2022**, *15*, (6), 2673-2710.
77. McDuffie, E. E.; Smith, S. J.; O'Rourke, P.; Tibrewal, K.; Venkataraman, C.; Marais, E. A.; Zheng, B.; Crippa, M.; Brauer, M.; Martin, R. V., A global anthropogenic emission inventory of atmospheric

- pollutants from sector- and fuel-specific sources (1970-2017): an application of the Community Emissions Data System (CEDS). *Earth System Science Data* **2020**, *12*, (4), 3413-3442.
78. Crippa, M.; Solazzo, E.; Huang, G. L.; Guizzardi, D.; Koffi, E.; Muntean, M.; Schieberle, C.; Friedrich, R.; Janssens-Maenhout, G., High resolution temporal profiles in the Emissions Database for Global Atmospheric Research. *Scientific Data* **2020**, *7*, (1).
79. Paasonen, P.; Kupiainen, K.; Klimont, Z.; Visschedijk, A.; van der Gon, H. A. C. D.; Amann, M., Continental anthropogenic primary particle number emissions. *Atmospheric Chemistry and Physics* **2016**, *16*, (11), 6823-6840.
80. Pozzer, A.; Anenberg, S. C.; Dey, S.; Haines, A.; Lelieveld, J.; Chowdhury, S., Mortality Attributable to Ambient Air Pollution: A Review of Global Estimates. *Geohealth* **2023**, *7*, (1).
81. Downward, G. S.; van Nunen, E. J. H. M.; Kerckhoffs, J.; Vineis, P.; Brunekreef, B.; Boer, J. M. A.; Messier, K. P.; Roy, A.; Verschuren, W. M. M.; van der Schouw, Y. T.; Sluijs, I.; Gulliver, J.; Hoek, G.; Vermeulen, R., Long-Term Exposure to Ultrafine Particles and Incidence of Cardiovascular and Cerebrovascular Disease in a Prospective Study of a Dutch Cohort. *Environmental Health Perspectives* **2018**, *126*, (12).

Fluorescent SPM



FeOx SPM

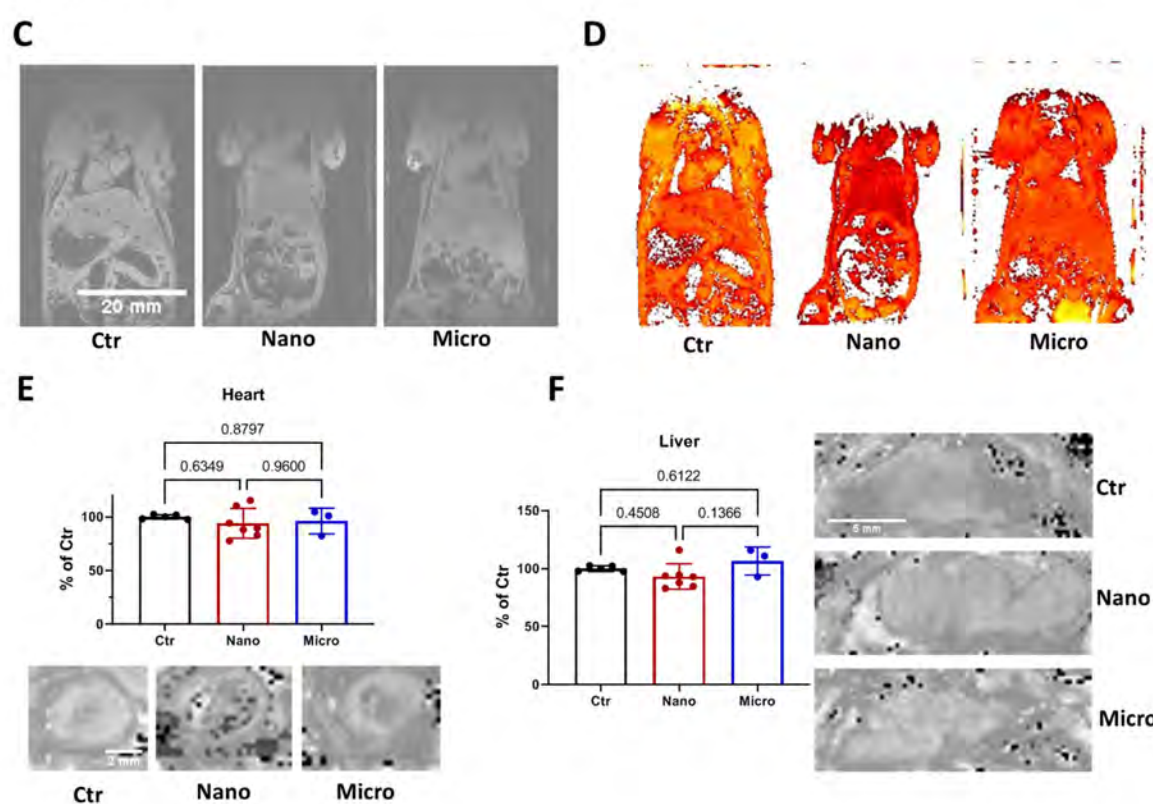


Figure 1. Distribution of particles with different size after inhalation in the mouse body.

Lungs of fluorescent nano and micro SPM exposed animals were subjected to fluorescence imaging (B), and the mean pixel intensity was recorded (A). Mice exposed to magnetic nano and micro SPM underwent magnetic resonance imaging (MRI) of the abdomen measuring T_2^* -relaxation maps. Representative T_2^* -weighted images (C) with the corresponding R_2^* parameter maps (D). Images of the heart (E) and liver (F) sections together with quantifications. The scale bar for B is 2 cm, for C and D is the same at 20 mm, for E is 2 mm and for F is 5 mm. Data are presented as mean \pm SEM from $n = 3 - 7$ animals per group. P values for individual comparisons are shown indicating statistical significance obtained by one-way ANOVA with Tukey's multiple comparison analysis.

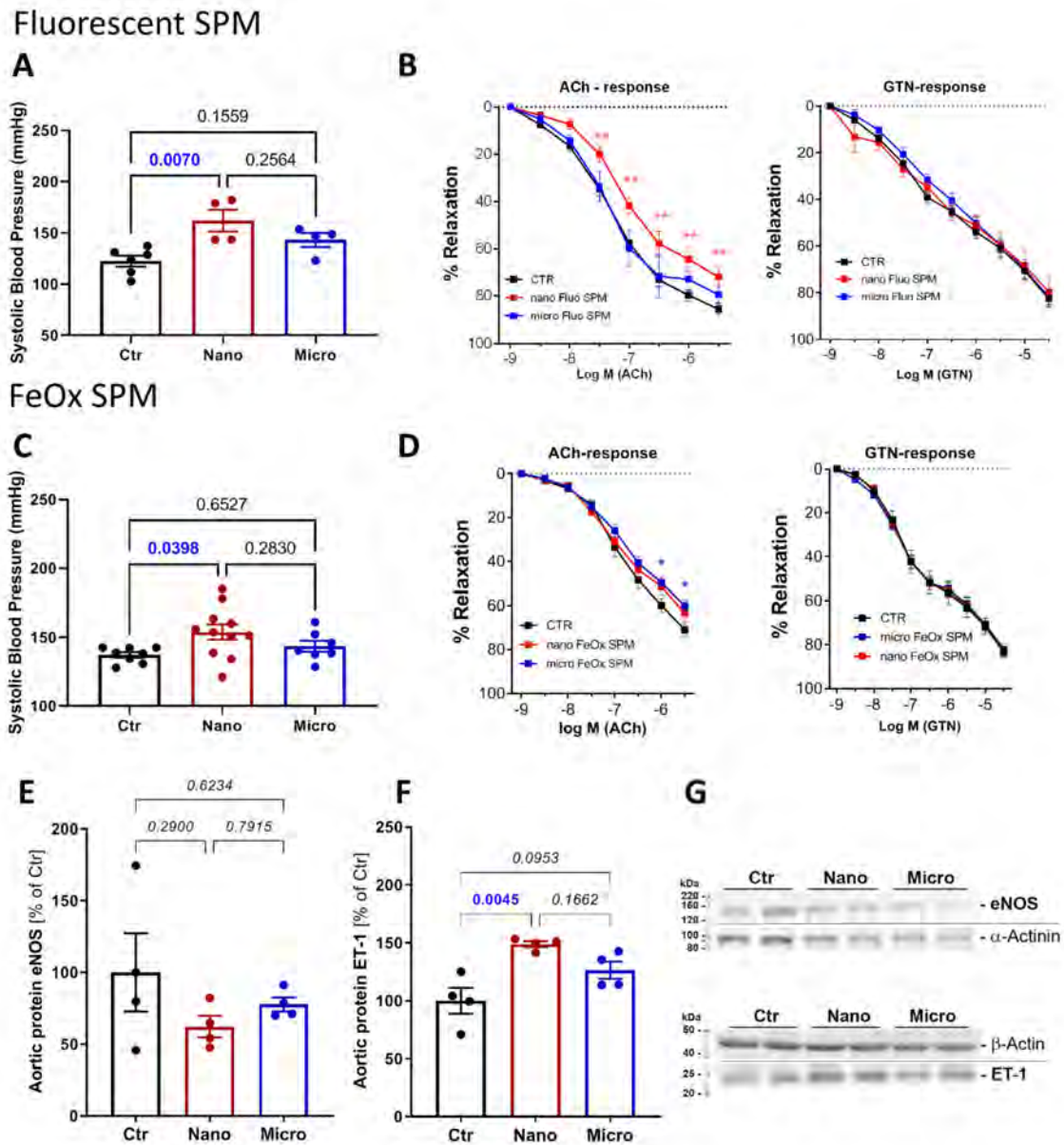


Figure 2. Effects of SPM different size on vascular function. Systolic blood pressure was measured in mice exposed to fluorescent SPM (A) and magnetic SPM (C). Vascular function was measured in isolated aortic rings of fluorescent SPM (B) and magnetic SPM (C). The endothelium-dependent relaxation in the presence of acetylcholine (ACh) and the endothelium-independent relaxation in the presence of nitroglycerin (GTN) are shown for both type of SPM exposure. Western blot quantifications for magnetic SPM-exposed mice aortic endothelial nitric oxide synthase (eNOS) (E) and endothelin 1 (ET-1) (F) expression levels are shown together with the representative blots (G). Data are presented as mean \pm SEM from aortic rings of $n = 4 - 9$ mice per group (B, D), or the mouse number is shown by jitter plots for other parameters ($n = 4 - 11$ mice per group). P values for individual comparisons are shown, indicating statistical significance, or asterisks are used: * ($p < 0.05$), ** ($p < 0.01$) obtained by one-way ANOVA with Tukey's multiple comparison analysis for A, C, E and F, and by two-way ANOVA with Tukey's multiple comparisons test for B and D.

Fluorescent SPM

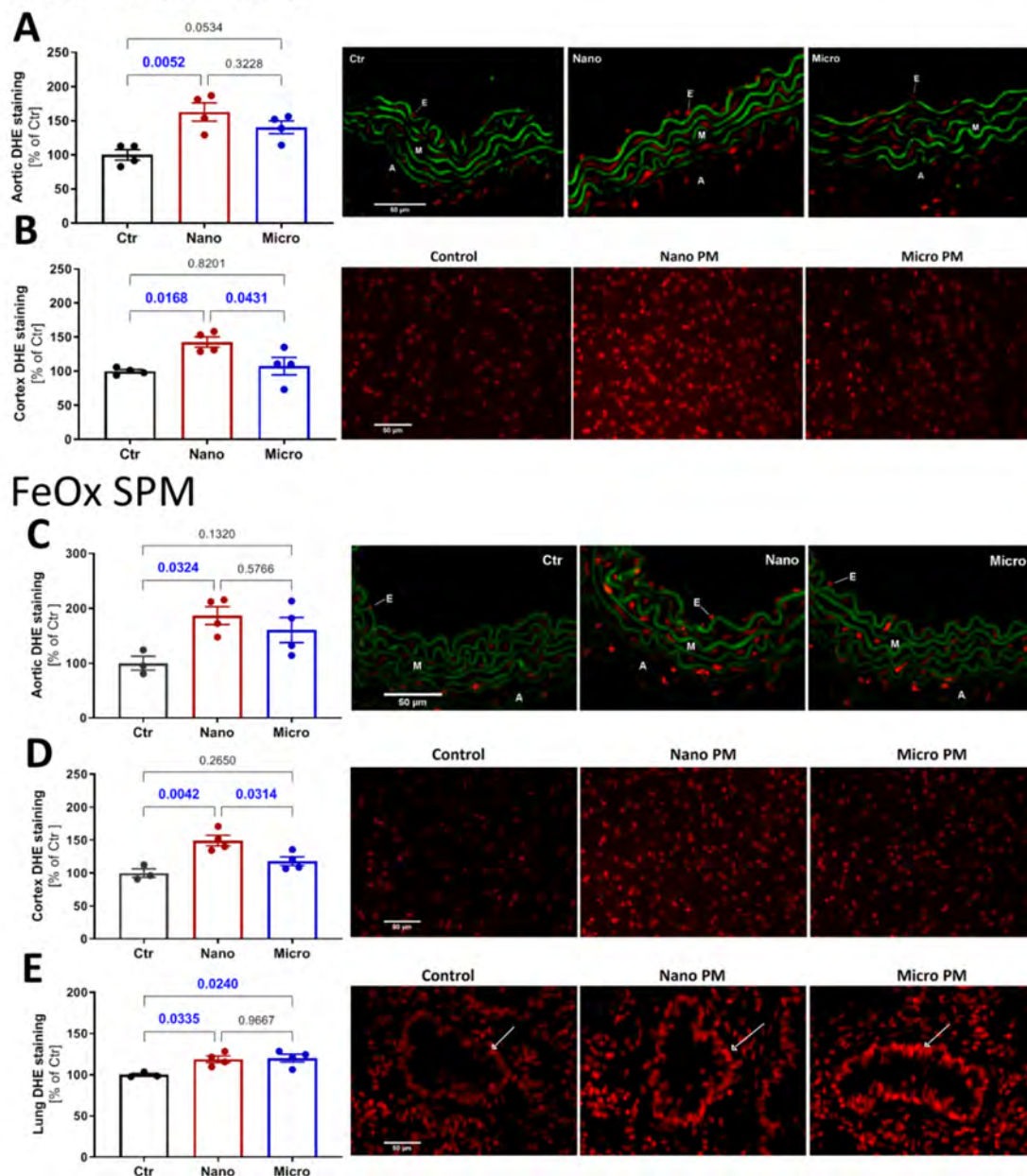


Figure 3. Effects of fluorescent SPM of different sizes on aortic, cortical and pulmonary oxidative stress. Dihydroethidium (DHE) fluorescence microtopography was used to assess the oxidative stress burden in different tissues. Quantification of oxidized DHE fluorescence in aortic (A) and cortical (B) tissue of fluorescent SPM exposed animals and in aortic (C), cortical (D), and pulmonary (E) tissue of magnetic SPM-exposed animals are shown together with representative image. Green color in panels A and C reflects the autofluorescence of the basal laminae. The arrows in panel E indicate the bronchioles. The scale bar for all images is the same at 50 μm . Data are presented as mean \pm SEM and the mouse number is shown by jitter plots ($n = 3 - 4$ mice per group). P values for individual comparisons are shown indicating statistical significance obtained by one-way ANOVA with Tukey's multiple comparison analysis.

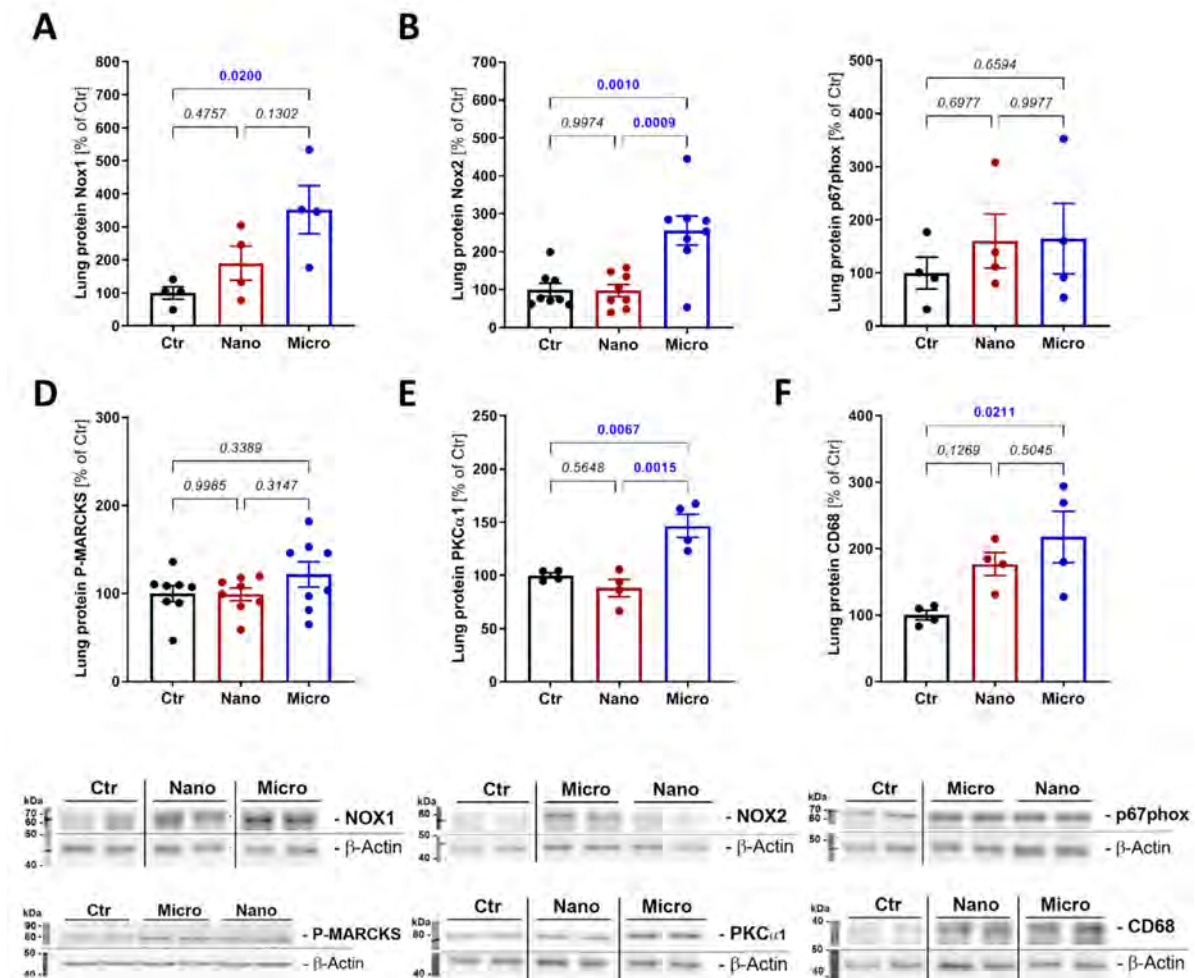


Figure 4. Effects of magnetic SPM with different sizes on pulmonary protein expression. Western blot analysis of the pulmonary NADPH oxidase subunits NOX1 (A), NOX2 (B) and p67phox (C), phosphorylated myristoylated alanine-rich C-kinase substrate (P-MARCKS) (D), protein kinase C alpha (PKC α 1) (E), and cluster of differentiation 68 (CD68) (F) are shown for the magnetic SPM exposed mice. Data are presented as mean \pm SEM, and the mouse number is shown by jitter plots ($n = 4 - 8$ mice per group). P values for individual comparisons are shown, indicating statistical significance obtained by one-way ANOVA with Tukey's multiple comparison analysis.

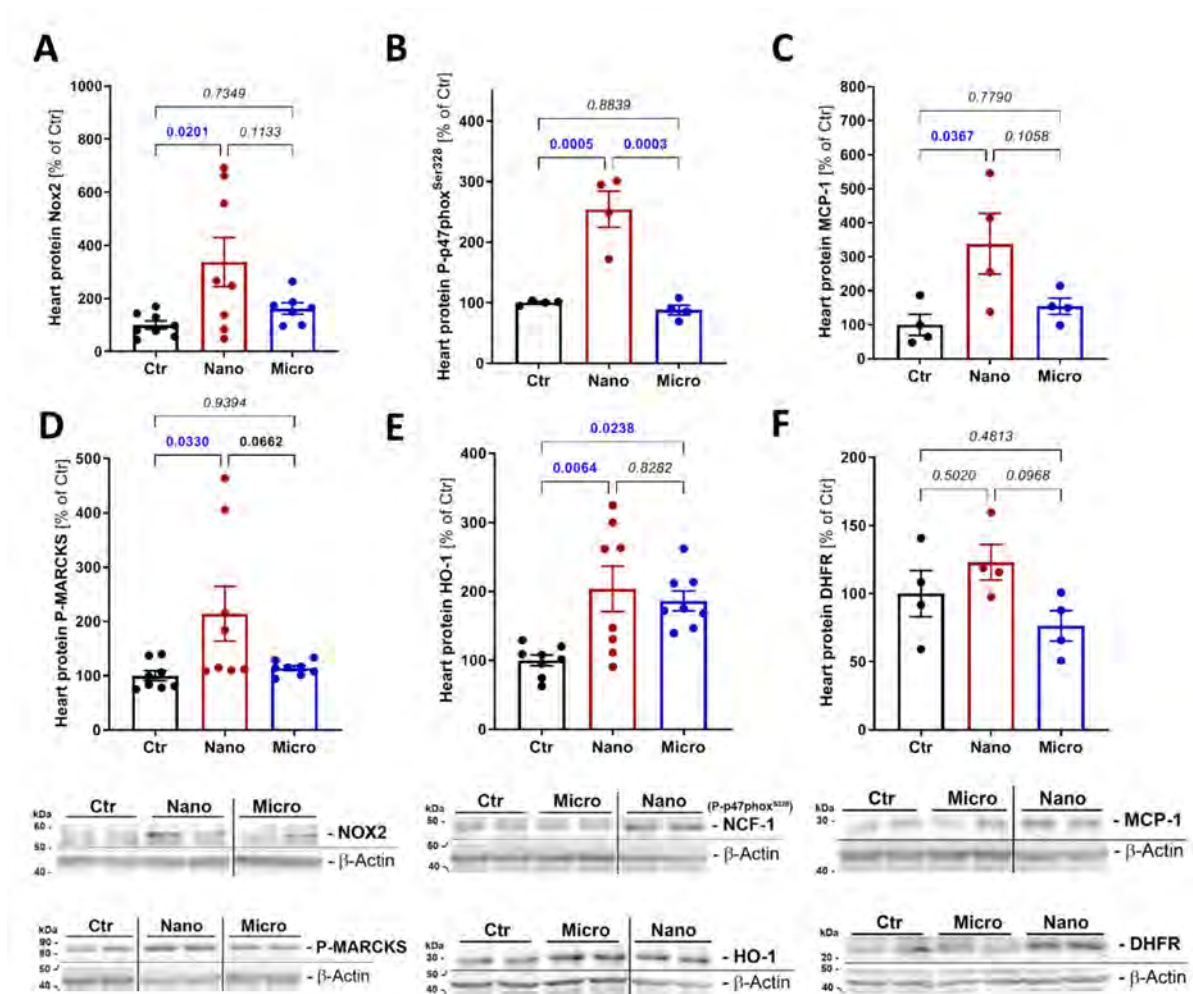


Figure 5. Effects of magnetic SPM with different sizes on cardiac protein expression. Western blot analysis of the pulmonary NADPH oxidase subunits NOX2 (A) and phosphorylated p47phox (NCF-1) (B), monocyte chemoattractant protein-1 (MCP-1) (C), phosphorylated myristoylated alanine-rich C-kinase substrate (P-MARCKS) (D), heme oxygenase-1 (HO-1) (E), and dihydrofolate reductase (DHFR) (F) are shown for the magnetic SPM-exposed mice. Data are presented as mean \pm SEM, and the mouse number is shown by jitter plots ($n = 4 - 8$ mice per group). P values for individual comparisons are shown, indicating statistical significance obtained by one-way ANOVA with Tukey's multiple comparison analysis.

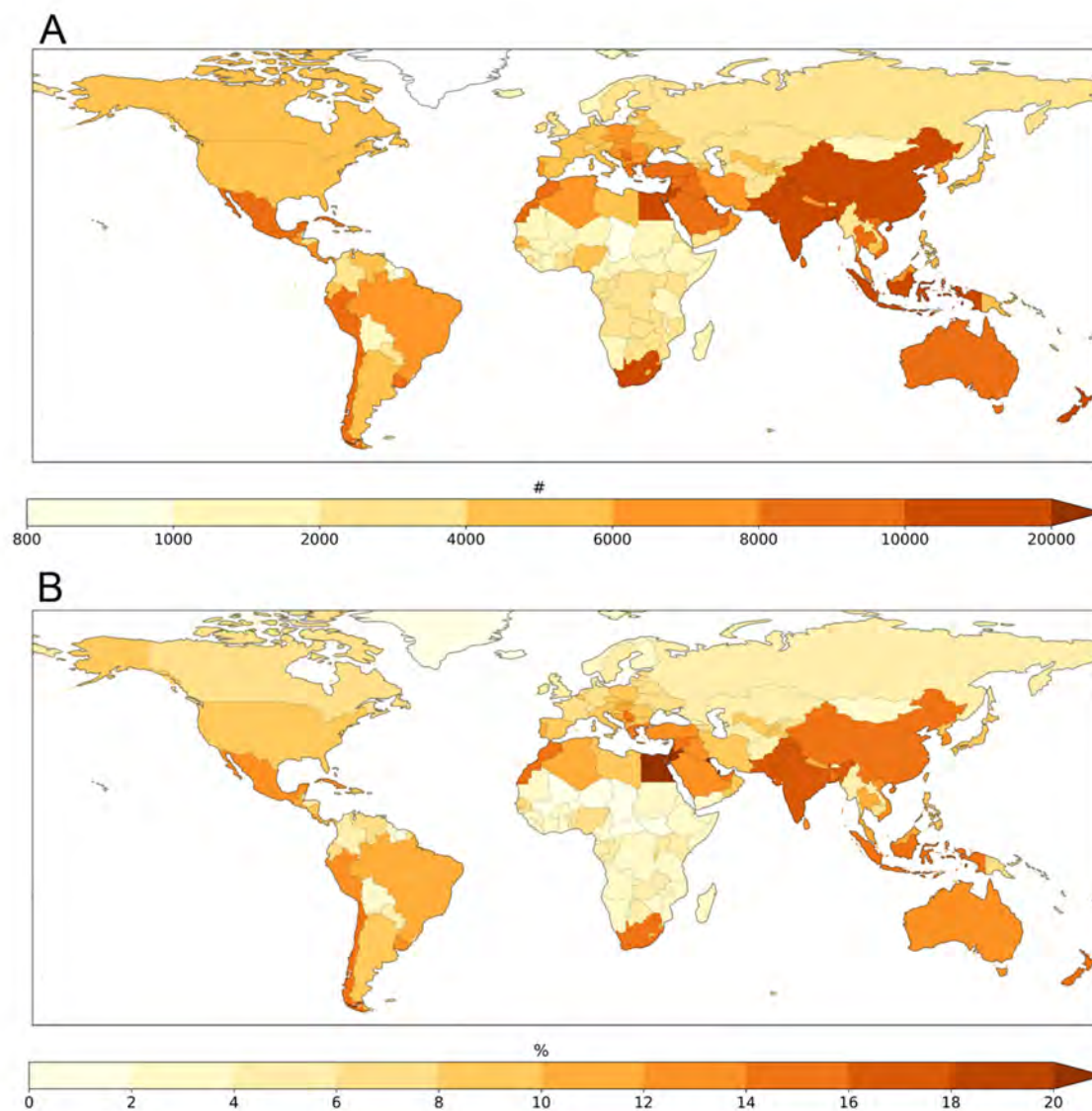


Figure 6. Annual and country average, population-weighted exposure to UFP. Particle concentrations are in numbers per cm³ (A). Country-average CVD incidence from UFP exposure relative to the total CVD incidence from all causes in percent (B).

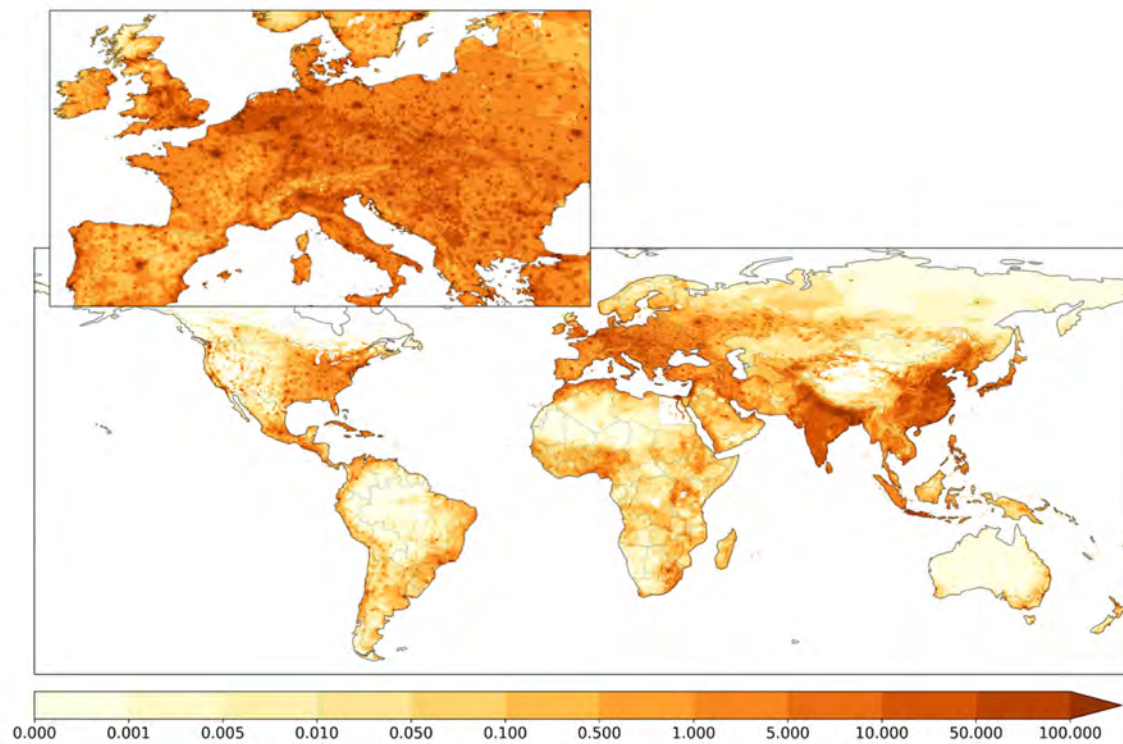


Figure 7. European and global, annual CVD incidence attributed to UFP. Units are the number of cases per surface area of 10 km×10 km.

- 157 7. Lu, Y.; Huang, J.; Neverova, N. V.; Nguyen, K. L., USPIOs as targeted contrast agents in cardiovascular magnetic
158 resonance imaging. *Curr Cardiovasc Imaging Rep* **2021**, *14*, (2).
- 159 8. Keselman, P.; Yu, E. Y.; Zhou, X. Y.; Goodwill, P. W.; Chandrasekharan, P.; Ferguson, R. M.; Khandhar, A. P.;
160 Kemp, S. J.; Krishnan, K. M.; Zheng, B.; Conolly, S. M., Tracking short-term biodistribution and long-term
161 clearance of SPIO tracers in magnetic particle imaging. *Phys Med Biol* **2017**, *62*, (9), 3440-3453.
- 162 9. Tan, H. H.; Fiel, M. I.; Sun, Q.; Guo, J.; Gordon, R. E.; Chen, L. C.; Friedman, S. L.; Odin, J. A.; Allina, J., Kupffer
163 cell activation by ambient air particulate matter exposure may exacerbate non-alcoholic fatty liver disease. *J*
164 *Immunotoxicol* **2009**, *6*, (4), 266-75.
- 165 10. Zhou, C.; Long, M.; Qin, Y.; Sun, X.; Zheng, J., Luminescent gold nanoparticles with efficient renal clearance.
166 *Angew Chem Int Ed Engl* **2011**, *50*, (14), 3168-72.
- 167 11. Alric, C.; Miladi, I.; Kryza, D.; Taleb, J.; Lux, F.; Bazzi, R.; Billotey, C.; Janier, M.; Perriat, P.; Roux, S.; Tillement,
168 O., The biodistribution of gold nanoparticles designed for renal clearance. *Nanoscale* **2013**, *5*, (13), 5930-9.
- 169 12. Li, X.; Wang, B.; Zhou, S.; Chen, W.; Chen, H.; Liang, S.; Zheng, L.; Yu, H.; Chu, R.; Wang, M.; Chai, Z.; Feng, W.,
170 Surface chemistry governs the sub-organ transfer, clearance and toxicity of functional gold nanoparticles in
171 the liver and kidney. *J Nanobiotechnology* **2020**, *18*, (1), 45.
- 172 13. Sadauskas, E.; Danscher, G.; Stoltenberg, M.; Vogel, U.; Larsen, A.; Wallin, H., Protracted elimination of gold
173 nanoparticles from mouse liver. *Nanomedicine* **2009**, *5*, (2), 162-9.
- 174 14. El-Sherbiny, I. M.; El-Baz, N. M.; Yacoub, M. H., Inhaled nano- and microparticles for drug delivery. *Glob Cardiol*
175 *Sci Pract* **2015**, *2015*, 2.
- 176 15. Meng, X.; Ma, Y.; Chen, R.; Zhou, Z.; Chen, B.; Kan, H., Size-fractionated particle number concentrations and
177 daily mortality in a Chinese city. *Environ Health Perspect* **2013**, *121*, (10), 1174-8.
- 178 16. Stolzel, M.; Breitner, S.; Cyrus, J.; Pitz, M.; Wolke, G.; Kreyling, W.; Heinrich, J.; Wichmann, H. E.; Peters, A.,
179 Daily mortality and particulate matter in different size classes in Erfurt, Germany. *J Expo Sci Environ Epidemiol*
180 **2007**, *17*, (5), 458-67.
- 181 17. Bergmann, M. L.; Andersen, Z. J.; Massling, A.; Kindler, P. A.; Loft, S.; Amini, H.; Cole-Hunter, T.; Guo, Y.; Maric,
182 M.; Nordstrom, C.; Taghavi, M.; Tuffier, S.; So, R.; Zhang, J.; Lim, Y. H., Short-term exposure to ultrafine
183 particles and mortality and hospital admissions due to respiratory and cardiovascular diseases in Copenhagen,
184 Denmark. *Environ Pollut* **2023**, *336*, 122396.
- 185 18. Cheng, H.; Saffari, A.; Sioutas, C.; Forman, H. J.; Morgan, T. E.; Finch, C. E., Nanoscale Particulate Matter from
186 Urban Traffic Rapidly Induces Oxidative Stress and Inflammation in Olfactory Epithelium with Concomitant
187 Effects on Brain. *Environ Health Perspect* **2016**, *124*, (10), 1537-1546.
- 188 19. Gonzalez-Maciel, A.; Reynoso-Robles, R.; Torres-Jardon, R.; Mukherjee, P. S.; Calderon-Garciduenas, L.,
189 Combustion-Derived Nanoparticles in Key Brain Target Cells and Organelles in Young Urbanites: Culprit Hidden
190 in Plain Sight in Alzheimer's Disease Development. *J Alzheimers Dis* **2017**, *59*, (1), 189-208.
- 191 20. Haghani, A.; Johnson, R.; Safi, N.; Zhang, H.; Thorwald, M.; Mousavi, A.; Woodward, N. C.; Shirmohammadi, F.;
192 Coussa, V.; Wise, J. P., Jr.; Forman, H. J.; Sioutas, C.; Allayee, H.; Morgan, T. E.; Finch, C. E., Toxicity of urban air
193 pollution particulate matter in developing and adult mouse brain: Comparison of total and filter-eluted
194 nanoparticles. *Environ Int* **2020**, *136*, 105510.